Using codispersion analysis to characterize spatial patterns in species co-occurrences

Using codispersion analysis to characterize spatial patterns in species co-occurrences

Hannah L. Buckley[1,2,*], Bradley S. Case[2,3], and Aaron M. Ellison[2]

[1]Department of Ecology, Lincoln University, Lincoln, Canterbury, 7647, New Zealand

[2]Harvard Forest, Harvard University, 324 North Main Street, Petersham, Massachusetts, 01366, USA

[3]Department of Informatics and Enabling Technologies, Lincoln University, Lincoln, Canterbury, 7647, New Zealand

*Author for correspondence: Hannah Buckley, Hannah.Buckley@lincoln.ac.nz

Abstract. Visualizing and quantifying spatial patterns of co-occurrence (i.e., of two or more species, or of species and underlying environmental variables) can suggest hypotheses about processes that structure species assemblages and their relevant spatial scales. Statistical models of spatial co-occurrence generally assume that underlying spatial processes are isotropic and stationary but many ecologically realistic spatial processes are anisotropic and non-stationary. Here, we introduce codispersion analysis to ecologists and use it to detect and quantify anisotropic and nonstationary patterns and their relevant spatial scales in bivariate co-occurrence data. Simulated data illustrated that codispersion analysis can accurately characterize complex spatial patterns. Analysis of co-occurrence of common tree species growing in a 35-ha plot revealed both positive and negative codispersion between different species; positive codispersion values reflected positive correlation in species abundance (aggregation), whereas negative codispersion values reflected negative correlation in species abundance (segregation). Comparisons of observed patterns with those simulated using two different null models showed that the codispersion of most species pairs differed significantly from random expectation. We conclude that codispersion analysis can be a useful exploratory tool to guide ecologists interested in modeling spatial processes.

Key words: *anisotropy, codispersion, co-occurrence, forest dynamics plot, spatial analysis, stationarity, variogram*

INTRODUCTION

A central inferential challenge for ecologists is the identification of mechanisms and operational scales of processes determining observed spatial patterns. We normally begin to address this challenge using spatial pattern analysis (e.g., Dale 1999, Cressie and Wikle 2011,

Wiegand and Moloney 2014). In particular, analysis and interpretation of patterns of co-occurrence of two or more species, or of individual species and environmental variables, are used routinely to identify relevant spatial scales and generate testable hypotheses about processes determining observed co-occurrence patterns (e.g., Wiegand and Moloney 2014).

Spatial patterns of co-occurring species often reflect the temporal integration of pairwise species associations, varying environmental conditions, and intra- and interspecific interactions (Dale 1999). For example, spatial patterns of locations and sizes of trees in a forest reflect the life history differences of the component species as well as the cumulative history of the stand: stochastic dispersal; small-scale environmental conditions for successful germination and establishment; self-thinning of once-dense groups of saplings and small trees; interspecific competition; loss of individuals to insects and disease; and ongoing environmental change. In many cases, environmental gradients dominate spatial patterns in forest stands, but the most widely-used spatial pattern analyses assume that underlying spatial processes of the analyzed spatial patterns are stationary (spatial processes are invariant under translation) and isotropic (invariant under rotation) (Dale 1999, Cressie and Wikle 2011). Although these assumptions are mathematically convenient, they are rarely true. Alternatives, such as wavelet and other spectral methods can be used to identify scales of variation in isotropic or anisotropic spatial data, but, some of these methods can analyze only limited types of ecological data (e.g., data collected on lattices: Deblauwe et al. 2012).

Codispersion analysis (Cuevas et al. 2013) is a new method for describing and visualizing complex spatial patterns of multiple co-occurring variables. In brief, codispersion quantifies covariation of two or more spatial patterns as a function of both spatial lag and direction (Cuevas et al. 2013). The analyzed spatial patterns may be any combination of point patterns, marked

point patterns (where we are interested in the spatial pattern of the marks, such as tree diameter), irregularly spaced plots, or rasters (contiguous grids); in the latter two cases, each plot or cell is assigned a single value, such as tree density or basal area. To date, codispersion analysis has been applied to only a limited number of datasets: photographic image analysis (Ojedat et al. 2012), the relationship between tree size and an underlying environmental gradient (Cuevas et al. 2013), bivariate temporal data (Vallejos 2012), and multivariate spectral data (Vallejos et al. 2015).

Cuevas et al. (2013) suggested that codispersion analysis may be useful to describe the pattern of covariation found in many different kinds of spatial ecological data, but it has not yet been used to analyze known (i.e., pre-determined) spatial patterns, nor have the results from observed patterns been evaluated against reasonable null expectations. Here, we describe how to apply codispersion analysis to species co-occurrence data. Using both simulated and real species co-occurrence data, we illustrate how the results can identify and quantify complex spatial patterns and spatial scales at which ecological processes may be operating. Results of codispersion analysis applied to simulated data illustrate the range of detectable patterns. We also show how to test for departure of observed codispersion from null models that (1) assume complete spatial randomness (CSR) in species co-occurrence or (2) fix the distances between points, but break the association between the two species by shifting one of the entire patterns randomly, treating the plot as a torus (toroidal shift null model).

METHODS

Examining codispersion between two or more spatial datasets depends on the precise locations at which measurements were made and the sampling grain of the measurements (i.e., the "support," *sensu* Dungan et al. 2002). If we are interested in point-wise codispersion between

two marked point patterns, the variables to be compared must be measured at exactly the same locations (e.g., beetles feeding on trees or the diameter and height of individual trees). In contrast, if the variables to be compared are measured at different spatial locations, the data need to be rescaled in one of two ways prior to analysis.

One way to rescale the data is convert the point patterns to small, identically-sized plots prior to analysis. If variables are measured at irregularly-spaced locations, they can be up-scaled to a common plot size; each "plot" is then considered to be a point with *x, y* coordinates equal to the center of the plot and with marks equal to some aggregate measure of the individuals within the "plot" (e.g., Cuevas et al. 2013). For example, if soil pH is measured at 100 random points and tree diameters are measured in a 20-m diameter circular plot around each of these points, then the average tree size in each plot can be used as the estimate of tree size at the point where soil pH was measured. Codispersion calculations then proceed as if the point patterns were measured at identical locations, but the "grain of inference" is the 20-m diameter plot. Alternatively, to compare the co-occurrence of two tree species in a large plot where, by definition, different individual trees cannot occupy identical point locations, we could first calculate the abundance of each species in individual contiguous subplots, i.e., one abundance raster for each species. Codispersion calculations then proceed as if the point patterns were measured at the centers of each of the subplots and the "grain of inference" is the size of each subplot (grid cell) in the rasters. In our worked examples, we use this latter, raster-based method.

A recipe for codispersion analysis of ecological data

To generate codispersion coefficients across a range of spatial scales (which we illustrate for rasterized data):

1. Generate three vectors of spatial lags (Fig. 1A). Two of these vectors of lags should be parallel to the *x* axis, one positive and one negative around zero ($-h_1$ to $+h_1$), up to one-fourth of the smallest plot dimension. The third vector of lags is parallel to the *y* axis, again increasing from the size of a raster up to one-fourth of the smallest plot dimension (h_2). For example, for a 500 × 700-m plot, the smaller dimension is 500 m, so the maximum of $|h_1|$ or $|h_2|$ is 500/4 = 125 m. This ensures an adequate sample size for calculating codispersion at the largest lag. The smallest lag size should be the grain size of the raster.
2. Apply a kernel function across all possible cell-wise distances for each lag to compute a variation surface for all lag distances and directions $\boldsymbol{h}$ (the two dimensions are defined by the $\{h_1, h_2\}$ coordinate pairs) for each dataset individually and the intersection of the two datasets. The way the kernel surfaces characterize spatial variation within and between datasets *X* and *Y* is controlled by specifying appropriate kernel bandwidth parameters $\boldsymbol{k} = \{k_X, k_Y, k_{XY}\}$ (Cuevas et al. 2013). If data have been rasterized, we recommend setting each element of $\boldsymbol{k}$ equal to the grid cell size of the raster.
3. Compute semi-variograms for each variable (γ_X, γ_Y), and the semi-cross-variogram (γ_{XY}) across all kernel-smoothed lag vectors $\boldsymbol{h}$ using a Nadaraya-Watson type estimator:

$$\hat{\gamma}_{XY_k}(\boldsymbol{h}) = \frac{\sum_{i=1}^{n}\sum_{j=1}^{n} K\left(\frac{\boldsymbol{h}-(\boldsymbol{s}_i-\boldsymbol{s}_j)}{k}\right)(X(\boldsymbol{s}_i)-X(\boldsymbol{s}_j))(Y(\boldsymbol{s}_i)-Y(\boldsymbol{s}_j))}{2\sum_{i=1}^{n}\sum_{j=1}^{n} K\left(\frac{\boldsymbol{h}-(\boldsymbol{s}_i-\boldsymbol{s}_j)}{k}\right)} \quad (1)$$

where $\boldsymbol{s}$ is the set of spatial locations and $K(\cdot)$ is a symmetric and strictly positive kernel function with bandwidth k_{XY} (Garcia-Soidán 2007, Cuevas et al. 2013).

4. Compute the empirical codispersion coefficient (Matheron 1965) for each lag ($\boldsymbol{h}$) as the semi-cross-variogram of the two variables ($\gamma_{XY}(\boldsymbol{h})$) normalized by the square root of the product of the semi-variograms of each of the two variables:

$$\hat{\rho}_{XY}(\boldsymbol{h}) = \frac{\hat{\gamma}_{XY}(\boldsymbol{h})}{\sqrt{\hat{\gamma}_X(\boldsymbol{h})\hat{\gamma}_y(\boldsymbol{h})}}. \quad (2)$$

where the formula for the empirical semi-variogram is:

$$\hat{\gamma}(\boldsymbol{h}) = \frac{1}{|N(\boldsymbol{h})|}\sum_{(i,j)\in N(\boldsymbol{h})}\left(Z(\boldsymbol{s}_i) - Z(\boldsymbol{s}_j)\right)^2, \quad (3)$$

In equations (2) and (3), $\boldsymbol{h}$ is the lag distance, $N(\boldsymbol{h})$ denotes the sets of pairs of observations, $\boldsymbol{s}$ is the set of spatial locations, and Z is the value of interest at a given location.

5. Plot the codispersion values for each spatial lag $\boldsymbol{h}$ (Fig. 1B). Positive codispersion values indicate positive covariation (aggregation) and negative codispersion values indicate negative covariation (segregation) for lag $\boldsymbol{h}$ with a given distance (in *x*,*y* space) and direction. Positive and negative lags on the *x*-axis refer to "looking right" (e.g., east) and "looking left" (e.g., west) within the plot, respectively. Positive lags on the *y*-axis refer to "looking up" (e.g., north) within the plot.

6. An appropriate set of null models should be selected to compare against the observed codispersion values. The choice of null model depends on the ecological question asked and the processes hypothesized to generate the observed spatial patterns. For instance, a CSR null model allows us to ask whether or not the observed pattern is spatially non-random, i.e., the species are distributed independently. Application of a toroidal shift null model asks whether the association between the species is non-random, given their univariate spatial patterns; thus, we are assessing their co-variation in space while excluding any effect of individual species' autocorrelation structures. Other, process-based null models (Wiegand and Moloney

145 2014) may be appropriate in certain circumstances, if sensible ideas about the processes
146 generating spatial patterns can be formulated (e.g., Wiegand et al. 2009).

147 *Illustrating codispersion analysis using simulations and real data*

148 We first generated and analyzed a range of bivariate spatial patterns (Fig. 2; a complete
149 set of simulated patterns is in Appendix A; pseudocode and accompanying R code is in the
150 Supplement). Because we were interested in comparing simulated results with observed data
151 from a large, gridded, forest inventory plot (see below), we simulated species abundance patterns
152 as a raster of 225 contiguous 20 × 20-m grid cells arrayed in a 300 × 300-m "plot". Abundance
153 values in grid cells were distributed either completely spatially randomly (CSR) among grid
154 cells, increasing or decreasing to the left side, right side, left or right top corners, or in one large
155 clump in the center of the plot. We analyzed a wide range of the possible pairs of these simulated
156 distributions (Appendix A).

157 Second, we analyzed all observed pairwise bivariate spatial patterns of the four most
158 abundant tree species in the Harvard Forest long-term forest dynamics plot (Orwig et al. 2015;
159 Figure 3A). This fully-censused 35-ha plot is part of the Smithsonian Tropical Research
160 Institute's Center for Tropical Forest Science – Forest Global Earth Observatory (CTFS-
161 ForestGEO) network of plots.[1] In this plot, a total of 116,227 woody stems > 1 cm diameter were
162 mapped, tagged, and measured between June 2010 and March 2014. The four most common
163 species, *Acer rubrum* L. (red maple, Sapindaceae), *Pinus strobus* L. (white pine, Pinaceae),
164 *Quercus rubra* L. (red oak, Fagaceae) and *Tsuga canadensis* (L.) Carrière (eastern hemlock,
165 Pinaceae), together comprise > 90% of the total basal area in the plot. Data are available from the
166 Harvard Forest data archive (Orwig et al. 2015).

[1] <http://www.forestgeo.si.edu>

We calculated the number of individuals of each of these four species within 20 × 20-m contiguous grid cells covering the 500 × 700-m plot (a total of 875 grid cells) and used these cell-level abundance data for all spatial analyses. We aggregated these data into 20 × 20-m cells because: this is the approximate canopy diameter of the dominant tree species in the Harvard Forest plot; 20 × 20 m (0.04 ha) is a common plot size used by foresters and ecologists to collect and analyze forest stand data (Kangas 2006); and a 20 × 20 m grid is the standard of collection and aggregation for ForestGeo data (Condit 1998).

We computed the codispersion of each pair of species at spatial lags ranging from 20 to 120 m. The maximum spatial lag equaled just under one-fourth of the length of the shortest side of the plot and was used to ensure adequate sample sizes for the largest spatial lag. To assess the significance of the observed codispersion patterns, we compared the observed codispersion values for each species pair calculated for each spatial lag and direction to values generated using two null models. The first was a CSR model, where one species distribution was fixed and the point locations of the other species were distributed completely spatially randomly across the plot. The second was a toroidal shift model, where the positions of trees were fixed, thus maintaining their autocorrelation structure, but the entire plot was shifted in a random direction and distance around a torus (Wiegand and Moloney 2014).

For each comparison, the null models were used to generate 199 new datasets for one of the species of each pair; 199 null simulations was a large enough number to confidently determine significant differences between observed and expected, and small enough to generate expected values on a desktop computer within a few days. Only one of the species pair needed to be randomized because this was enough to break their spatial association, allowing us to test the significance of their co-variation. The observed codispersion values at each spatial lag were then

compared to the vector of codispersion values at the same spatial lags and directions under each null model to estimate tail probabilities; if the observed value was greater than or equal to the 195th value or less than or equal to the 5th value, we deemed it to be significantly different from expected (i.e., a two-tailed test; $P < 0.05$). Finally, we calculated the Type I error rate of the CSR and toroidal shift null models by comparing the observed codispersion between two CSR simulated patterns (Appendix B) to values generated under the CSR and toroidal shift models.

RESULTS

Simulations

Codispersion analysis accurately detected both positive and negative covariation in abundance in simulated bivariate spatial patterns (Fig. 2). For cases in which we simulated no strong covariation between two species (i.e., at least one "species" was CSR), codispersion values at all lags were around zero (Fig. 2A; Appendix A). When the two species were strongly segregated or aggregated (i.e., negative or positive covariance, respectively, between them; Fig. 2B-2C), the codispersion values were similarly highly negative or positive. When the patterns of abundance of the two species were strongly anisotropic in the east-west direction (the *x* [horizontal] dimension of the plot), such that in some areas of the plot the species were aggregated and in other areas they were segregated (Fig. 2D-2F), the analysis illustrated the anisotropy by having different patterns for positive and negative lags on the *x*-axis of the codispersion graph. Positive codispersion values reflected lags and directions over which species were both either increasing or decreasing in abundance (Fig. 2D-2F). In contrast, negative values of codispersion represented lags and directions for which the abundances of the two species were negatively correlated, e.g., one species was high in abundance when the other was low. Rotating the species' patterns illustrated that the method was sensitive to the orientation of the plot

(Compare Fig. 2B and 2C). Analysis of the mirrored reflection of the patterns illustrated that identical results were obtained for positive and negative lags in the *y* direction (compare Figs. 2E and 2F). For both the CSR and toroidal shift null models, none of the observed codispersion values from the two CSR patterns were significantly different from that expected under either model at the 5% level, indicating a Type I error rate ≤ 5% for both null models (Appendix B).

Real data

Empirical semi-variograms illustrated that spatial autocorrelation of *P. strobus* in the 35-ha forest dynamics plot was apparent up to lags of approximately 180 m, but that abundances of the other three species were autocorrelated at scales of at least 300 m (variograms showed a linear trend, with no sill; Fig. 3B). *Tsuga canadensis*, the dominant species, negatively co-varied with (i.e., was spatially segregated from) the three other species (Fig. 4). This species showed weak anisotropy in its covariation with *Q. rubra* and *A. rubrum*, as indicated by different values of the codispersion coefficient on the right and left-hand sides of the codispersion graph, but not with *P. strobus*. In contrast, the three sub-dominant species all positively co-varied (were aggregated) at most spatial lags; the positive codispersion was strongest between *Q. rubra* and *A. rubrum* (Fig. 4). The observed codispersion patterns largely were significantly different from those expected under the two null models, except for *P. strobus* and *Q. rubra*, which showed only weak positive covariation (Fig. 4). Because the toroidal shift null model maintained the autocorrelation structure of the individual species' patterns while breaking their bivariate spatial association, observed codispersion values were significantly different from null expectation at a smaller number of lags than we observed with the CSR model (Fig. 4).

DISCUSSION

Codispersion analysis is an effective method for quantifying and visualizing the pairwise covariation of two or more variables in space (Vallejos et al. 2015). One of the key benefits of this method is that it gives a 2-D graph illustrating the sign (positive or negative), magnitude, scale, and direction of covariation between two species. This information is especially useful for choosing appropriate models for subsequent inference about underlying spatial processes.

Most methods used to model spatial data assume that the data are stationary (but see Wiegand et al. 2007, Getzin et al. 2008). The "strong" form of spatial stationarity is the situation in which both the joint distribution of the data is invariant when the pattern is moved (translated) through space. For ecological data, this assumption is rarely, if ever, true. A weaker form of spatial stationarity, "second-order stationarity," assumes that only the mean, variance, and covariance must be stationary (Vieira et al. 2010). Even this assumption is rarely satisfied. However, most spatial statistical methods can be used if the data meet the assumption of the "intrinsic hypothesis:" that the mean and the semi-variance of the distribution are dependent only on distance between points, not on their location; i.e., there is no underlying large-scale spatial "trend" in the data (Vieira et al. 2010).

A common way to determine if there is spatial trend in the data is to compare the semi-variograms between raw and adequately detrended data: raw data with a spatial trend will have a semi-variogram that lacks a sill, whereas the semi-variogram of data without a spatial trend will have an obvious and stable sill (Vieira et al. 2010). However, simply detrending data and comparing semi-variograms does not identify directionality in the data. In contrast, codispersion plots illustrate distances and directions at which significant spatial covariance occur.

In our examples, codispersion plots correctly detected isotropic and anisotropic positive and negative spatial covariation in simulated abundances of two species on a grid for a variety of ecologically interpretable patterns (Fig. 1; Appendix A). Analysis of pairwise co-occurrences of the abundances of forest tree species in a 35-ha plot (Fig. 3) also showed that codispersion analysis could detect subtle variation in spatial co-occurrences among species. Comparisons of observed values with those obtained from repeated realizations of null models also could be used to evaluate the statistical significance of observed patterns of anisotropic spatial covariance.

We emphasize that codispersion analysis can only detect and illustrate covariation in species distribution patterns; like a semi-variogram, a codispersion graph it is not explicitly designed to reveal the processes that gave rise to the observed patterns. For instance, there are at least two possible reasons that species' distributions can co-vary in space: (1) interactions that lead to aggregation or segregation; or (2) similarity or differences in species' habitat preferences or other underlying (and unmeasured) variables, such as soil nutrients. As shown by the simulations (e.g., Fig. 1D), patterns that are caused by different spatial processes will show high codispersion if they co-vary spatially. However, comparison of observed codispersion to that expected under different null models can help determine the nature of the observed spatial pattern and how to develop predictive process models. For example, *P. strobus* and *Q. rubra* showed no significant codispersion at all but the largest spatial scales under either the CSR or toroidal shift null model. This result suggests that these data meet the assumption of second-order stationarity and that process models to describe their covariance could proceed without detrending the data. In contrast, all other pairs of species showed some significant codispersion relative to the toroidal shift model, suggesting that at best, process models of their covariance could lend support to the intrinsic hypothesis, not second-order stationarity.

279 The choice of null models also is critical in any description of spatial pattern. The CSR
280 null model, as we applied it, did not account for tree size in randomly rearranging their positions,
281 so it is possible that trees in the null patterns were closer than is realistic, given their size.
282 Further, the toroidal shift model can lead to artificial significance if large-scale clustering occurs
283 at the plot edges, creating edge effects in the null realizations (Wiegand and Moloney 2014, pp
284 365). In the case of the data from the Harvard Forest's 35-ha forest dynamics plot, variable land-
285 use history within the plot area precluded using a model based on a simple spatial process, such
286 as a Thomas cluster process, which would assume spatial homogeneity in the plot. Future
287 research should pursue more alternative null models; recent research suggests that spectral
288 randomization methods (e.g. Deblauwe et al. 2012, Wagner and Dray 2015) and pattern
289 reconstruction (Wiegand and Moloney 2014, pp 368) may be useful approaches to this problem.
290 The key consideration when applying a null model to a spatial pattern is that we understand the
291 process being tested by the model; this may not be trivial for more complex null models.
292 When using codispersion analysis with any null model, there are three technical issues
293 that are important to keep in mind. First, a maximum lag distance should be selected that is not
294 more than one-quarter of the smallest dimension of the plot. This ensures that an adequate
295 number of pairs at all combinations of lags (especially the maximum lag) and directions for
296 calculating the codispersion coefficient are available.
297 Second, the choice of bandwidth for the kernel function is critical. By default, our code
298 (based on Cuevas et al. 2013) uses the same kernel for both variables and their intersection (the
299 cross-variogram). However, if the spatial variation in the two variables differs substantially, it
300 may be appropriate to select different bandwidths for the different variables. A sensible value for
301 the kernel bandwidth should be selected that is no smaller than the grain size (support) of the

data and not so large that it smooths across lags (which results in no differentiation across the codispersion graph). Cuevas et al. (2013) recommend using an optimization method to select appropriate bandwidth parameters for the kernel function. More easily, the range of the univariate variograms and bivariate cross-variogram (if they exist) might be used to select an appropriate bandwidth for each variable and their covariance. We note, however, that detrending the data to obtain stable variograms with sills (as suggested by Vieira et al. 2010) prior to running codispersion analysis can be expected to eliminate the pattern that codispersion aims to detect (Appendix C).

Clearly, the kernel bandwidth will differ if raw point-pattern data are used or if the data are rasterized. If the observations are of individual locations in space (i.e., a point pattern), the initial selection of the scale at which the data could be rasterized (or not) should be determined based on biological considerations. If all variables are measured at identical points, no rasterization is necessary. However, in many ecological datasets, individuals of two or more different species do not co-occur at identical locations (due to physical constraints or the scale of sampling), so rasterizing species co-occurrences makes sense. Note, however, that rasterizing a point pattern so that grid cells include ≥ 1 observation is equivalent to applying a uniform bivariate kernel with bandwidth equal to the width of a grid cell. Thus, when calculating codispersion values as illustrated in Fig. 3, we set the bandwidth parameter to 20 m so as to not re-smooth the data any further than they had already been rasterized.

Finally, codispersion analysis is particularly useful for examining anisotropic patterns and processes. As a result, the orientation of the data matters. The *x* and *y* dimensions of the values in the codispersion graphs (Figs. 1, 3) describe lags in the “left”, “right”, and “up” directions, and anisotropy is illustrated in most detail across the *x* dimension (see also Appendix

1). Therefore, we recommend that the data be oriented in a manner that reflects the directionality of patterns of particular interest, or, that the pattern is rotated and analyzed in both directions. In this way, interesting patterns are more likely to be identified and used to suggest new and testable ecological hypotheses. Future research also should directly compare the ability of this method to detect complex multivariate spatial patterns with that of other methods, including spectral analysis (Deblauwe et al. 2012), geographically weighted regression (Fotheringham et al. 2002), and Moran eigenvector maps (Wagner and Dray 2015).

ACKNOWLEDGMENTS

We thank Michael Lavine, Ronny Vallejos, Nick Gotelli, and the Harvard Forest Lab Group for valuable discussions of these ideas; three anonymous reviewers and Helene Wagner for constructive comments on the manuscript; Dave Orwig for use of the Harvard Forest ForestGeo plot data; and Thorsten Wiegand, Adrian Baddeley, Ege Rubak, Matt Lau, and Samuel Case for help with coding and computation. HLB and BSC were supported by a Charles Bullard Fellowship at Harvard Forest while conducting this research. AME was supported by NSF grant 12-37491. This paper is a contribution of the Harvard Forest LTER program.

LITERATURE CITED

Condit, R. 1998. Tropical forest census plots: methods and results from Barro Colorado Island, Panama and a comparison with other plots. Springer-Verlag, Berlin, Germany.

Cressie, N., and C. K. Wikle. 2011. Statistics for spatiotemporal data. John Wiley and Sons, Hoboken, New Jersey.

Cuevas, F., E. Porcu, and R. Vallejos. 2013. Study of spatial relationships between two sets of variables: a nonparametric approach. Journal of Nonparametric Statistics 25:695–714.

Dale, M. R. T. 1999. Spatial pattern analysis in plant ecology. Page 326. Cambridge University Press, Cambridge, UK.

Deblauwe, V., P. Kennel, P. Couteron. 2015. Testing pairwise association between spatial autocorrelated variables: A new approach using surrogate lattice data. PLoS ONE 7(11): e48766.

Dungan, J. L., J. T. Perry, M. R. T. Dale, P. Legendre, S. Citron-Pousty, M.-J. Fortin. 2002. A balanced view of scale in spatial statistical analysis. Ecography 25: 626-640.

García-Soidán, P. 2007. Asymptotic normality of the Nadaraya–Watson semivariogram estimators. Test 16:479–503.

Fotheringham, S. A., C. Brunsdon and M. Charlton. 2002. Geographically weighted regression: The analysis of spatially varying relationships. John Wiley & Sons, Chichester, England.

Kangas, A. 2006. Mensurational aspects. Pages 53-64 *in* A. Kangas and M. Maltamo, editors. Forest inventory: methodology and applications. Springer, Dordrecht, The Netherlands.

Matheron, G. 1965. *Les variables régionalisées et leur estimation.* Masson, Paris, France.

Ojeda, S., R. Vallejos, and P. Lamberti. 2012. Measure of similarity between images based on the codispersion coefficient. Journal of Electronic Imaging 21:023019–1.

Orwig, D., D. Foster and A.M. Ellison. 2015. Harvard Forest CTFS-ForestGEO Mapped Forest Plot since 2014. http://harvardforest.fas.harvard.edu:8080/exist/apps/datasets/showData.html?id=hf253

Ribeiro, P. J., Jr., and P. J. Diggle. 2001. geoR: a package for geostatistical analysis. R-News 1:2.

Vallejos, R. 2012. Testing for the absence of correlation between two spatial or temporal sequences. Pattern Recognition Letters 33:1741–1748.

Vallejos, R., A. Mallea, M. Herrera, and S. Ojeda. 2015. A multivariate geostatistical approach for landscape classification from remotely sensed image data. Stochastic Environmental Research and Risk Assessment 29:369–378.

Vieira, S. R., J. R. Porto de Carvalho, M. B. Ceddia, A. P. González. 2010. Detrending non stationary data for geostatistical applications. Bragantia 69: 1-8.

Wagner, H. H. and S. Dray. 2015. Generating spatially-constrained null models for irregular spaced data using Moran spectral randomization methods. Methods in Ecology and Evolution. In press. DOI: 10.1111/2041-210X.12407.

Wiegand, T., C. V. S. Gunatilleke, I. A. U. N. Gunatilleke, and A. Huth. 2007. How individual species structure diversity in tropical forests. Proceedings of the National Academy of Sciences 104(48): 19029-19033.

Wiegand, T., I. Martinez, and A. Huth. 2009. Recruitment in tropical tree species: Revealing complex spatial patterns. American Naturalist 174: E106-E140.

Wiegand, T., and K. A. Moloney. 2014. A handbook of spatial point pattern analysis in ecology. CRC Press, Boca Raton, Florida.

APPENDIX A. Complete results of simulations

APPENDIX B. Results for estimating the null model type I error rates

APPENDIX C. Effects of detrending on codispersion analysis

SUPPLEMENT. Psuedocode and R code for all analyses and figures

Figure legends

Figure 1. (A) Illustration of the generation of spatial lags in three directions for two rasterized surfaces (Datasets A and B) used as input to codispersion analysis. (B) A codispersion plot. The color of each cell is the value of the codispersion coefficient of two variables for each given spatial lag $\boldsymbol{h}$ and direction in x,y space.

Figure 2. Simulated species co-occurrence patterns on 20 × 20-m grids in 300 × 300-m plots and their resultant codispersion graphs. In each case, the colors on the codispersion graphs on the left are scaled to the range of values for that plot and those on the right are scaled from –1 to +1. The mean (standard deviation) codispersion values for each analysis were (A) 0.02 (0.02), (B) -0.77 (0.21), (C) -0.87 (0.09), (D) 0.38 (0.48), (E) -0.28 (0.56) and (F) -0.28 (0.56).

Figure 3. Observed (A) point patterns and (B) semi-variograms for the four most abundant species in the Harvard Forest 35-ha forest dynamics plot, calculated using species' abundances in 20 × 20-m rasters. In (A), the sizes of the symbols are scaled to each tree's DBH: diameter measured at breast height (1.3-m above ground).

Figure 4: Observed codispersion values and their significance (red) or not (blue) when compared to null expectation for bivariate co-occurrence data from all species pairs of the four most common tree species in the Harvard Forest 35-ha forest dynamics plot, calculated using species' abundances in 20 × 20-m grid cells. Scaled (–1 to +1) codispersion graphs are shown with 0.1-unit contours. On the left, the mean codispersion values for each codispersion graph (standard deviation) are given for each species pair. Significance of codispersion values in each grid cell were calculated by comparing the observed value with 199 codispersion values from a CSR null model and a toroidal shift null model; if the

observed value was greater than or equal to the 195th value or less than or equal to the 5th value, the cell was labelled as significant.

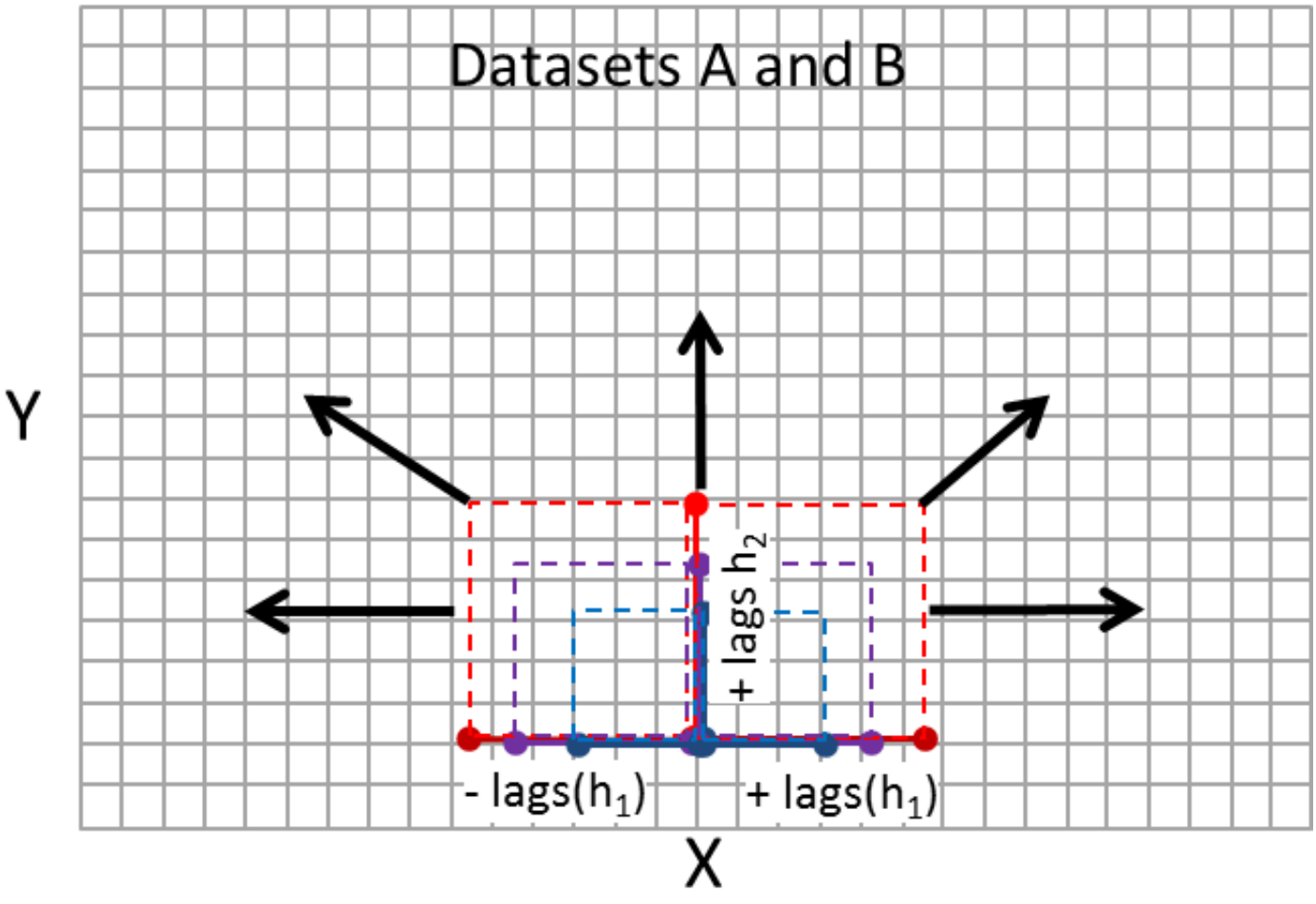
Datasets A and B
Y
+ lags h_2
- lags(h_1)
+ lags(h_1)
X

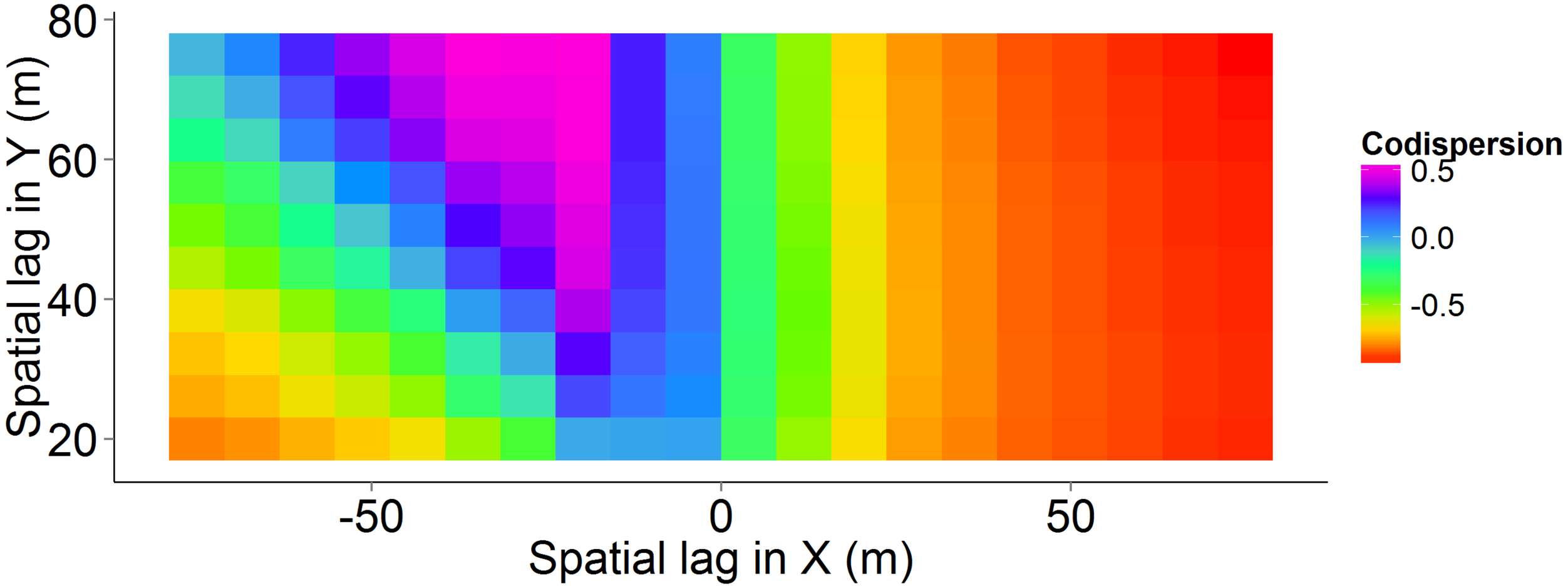
Spatial lag in Y (m)
80
60
40
20
-50
0
50
Spatial lag in X (m)
Codispersion
0.5
0.0
-0.5

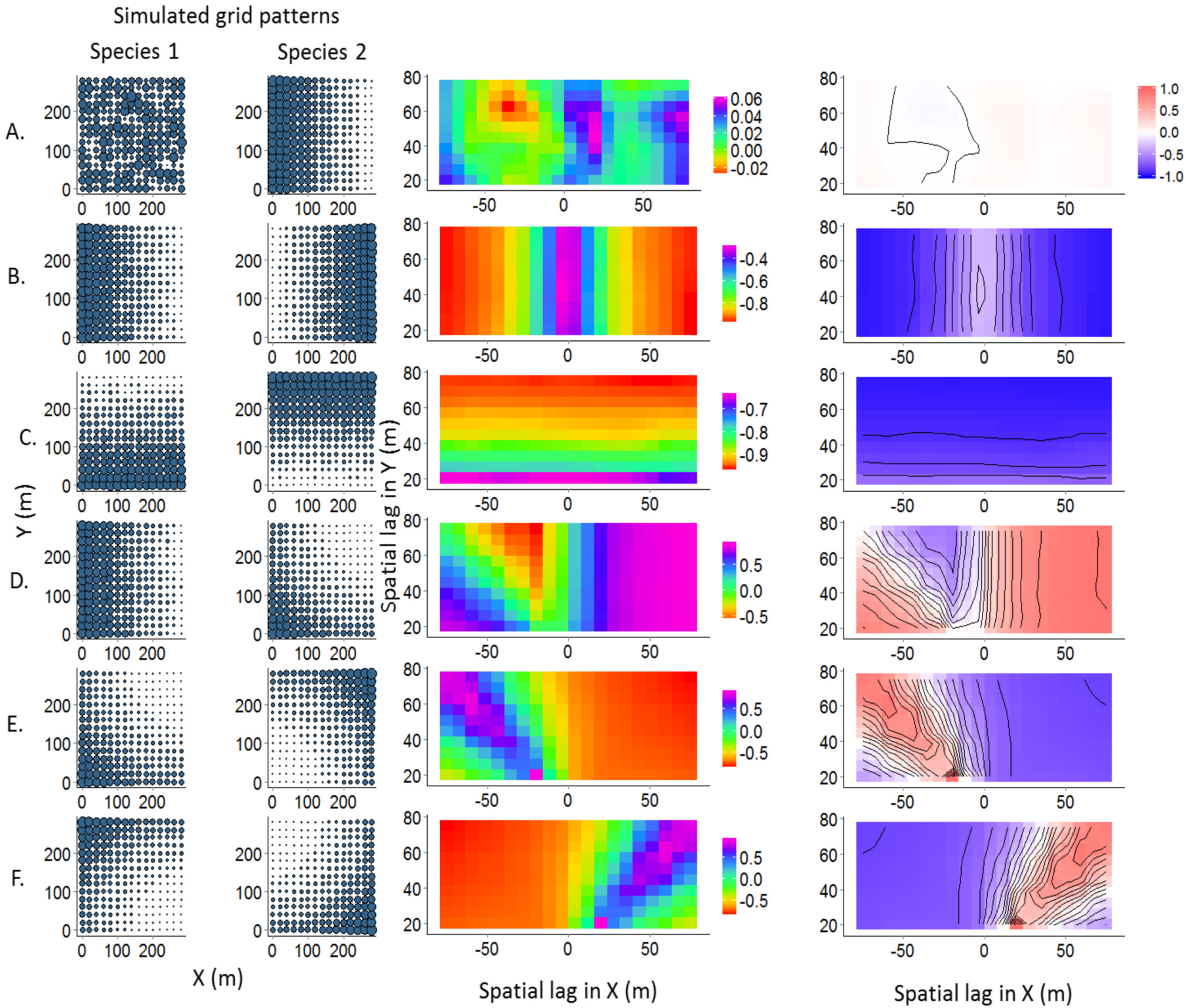
Simulated grid patterns
Species 1
Species 2
A.
B.
C.
D.
E.
F.
Y (m)
X (m)
Spatial lag in Y (m)
Spatial lag in X (m)
Spatial lag in X (m)
0.06
0.04
0.02
0.00
-0.02
-0.4
-0.6
-0.8
-0.7
-0.8
-0.9
0.5
0.0
-0.5
0.5
0.0
-0.5
0.5
0.0
-0.5
1.0
0.5
0.0
-0.5
-1.0

Acer rubrum

Pinus strobus

Quercus rubra

Tsuga canadensis

Y (m)

0
100
200
300
400
500

X (m)

0
200
400
600

DBH

25
50
75

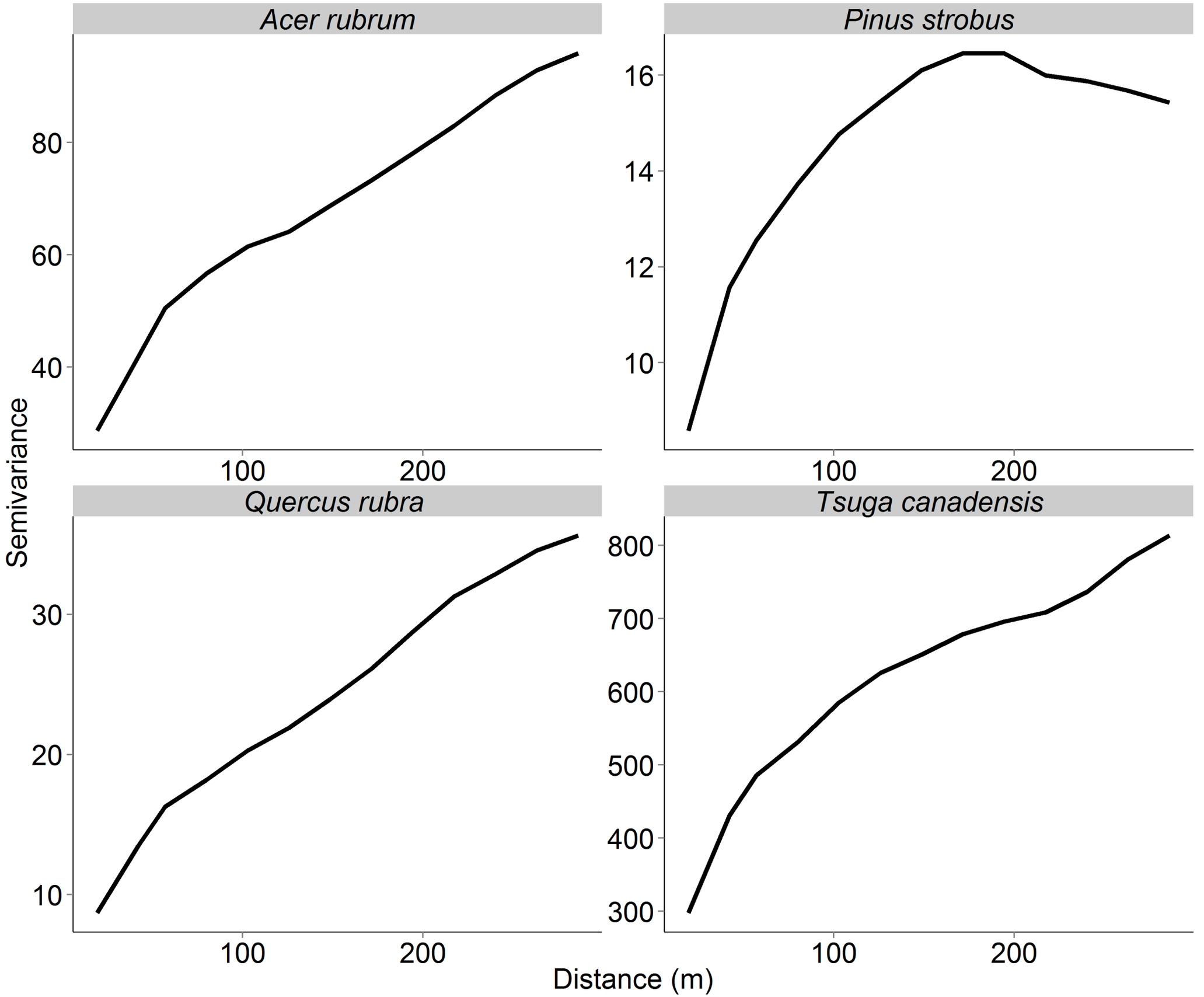
Acer rubrum
Pinus strobus
Quercus rubra
Tsuga canadensis
Semivariance
Distance (m)
40
60
80
10
12
14
16
10
20
30
300
400
500
600
700
800
100
200

CSR

Toroidal shift

Observed

Obs.– Exp.

Sig.

Obs.– Exp.

Sig.

Tsuga canadensis vs.
Pinus strobus
Mean = -0.28 (0.08)

Tsuga canadensis vs.
Quercus rubra
Mean = =-0.13 (0.04)

Tsuga canadensis vs.
Acer rubrum
Mean = -0.18 (0.09)

Pinus strobus vs.
Quercus rubra
Mean = 0.07 (0.03)

Pinus strobus vs.
Acer rubrum
Mean = 0.18 (0.04)

Quercus rubra vs.
Acer rubrum
Mean = 0.28 (0.11)

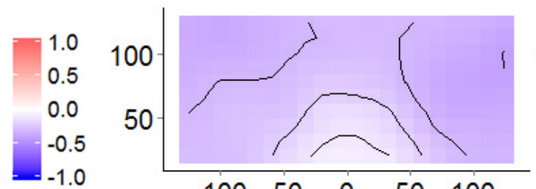

APPENDIX A

Codispersion results, presented as codispersion graphs with scaled and unscaled colors, from all simulated bivariate codispersion analyses. See Supplement 1 for R code to generate these graphs.

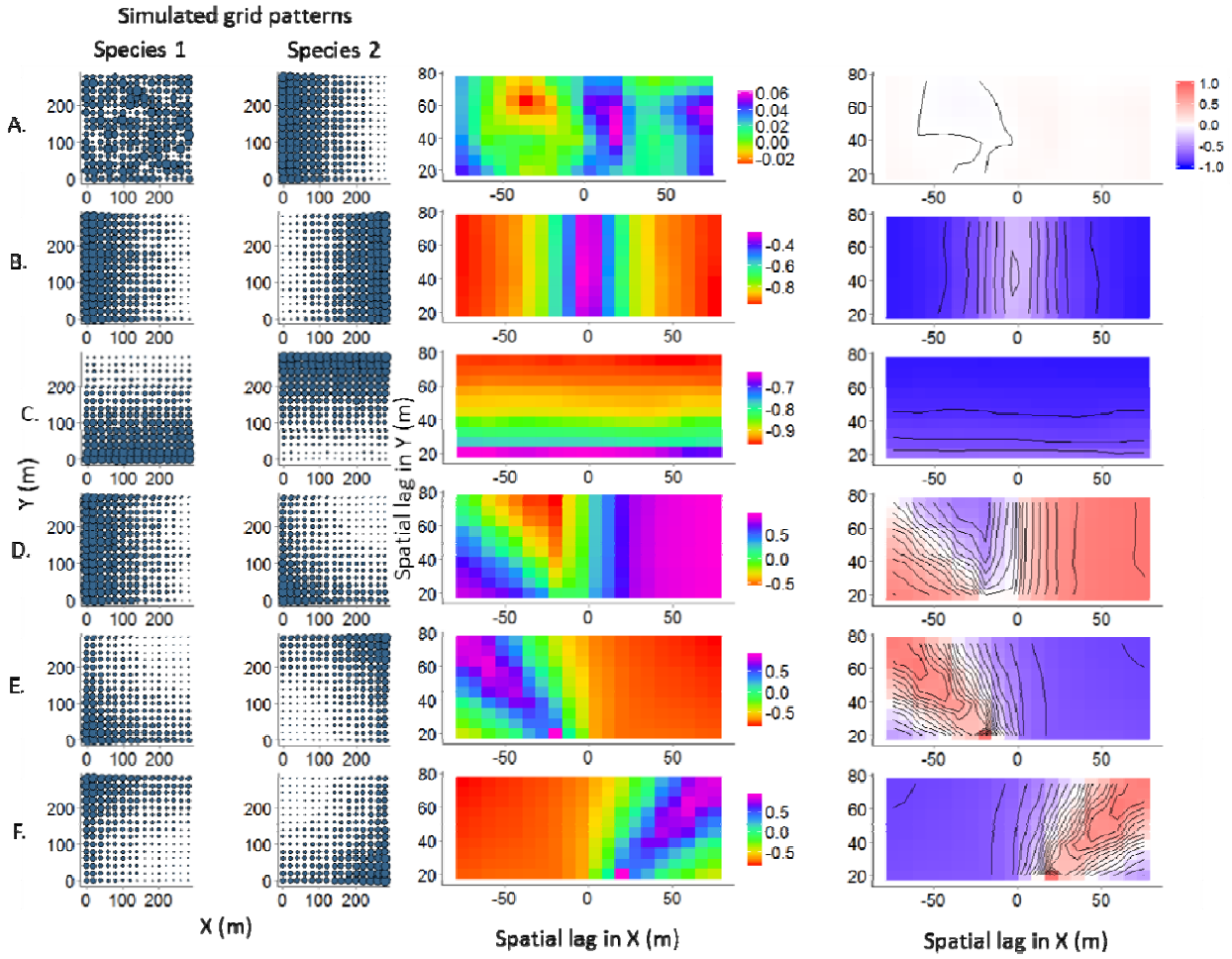

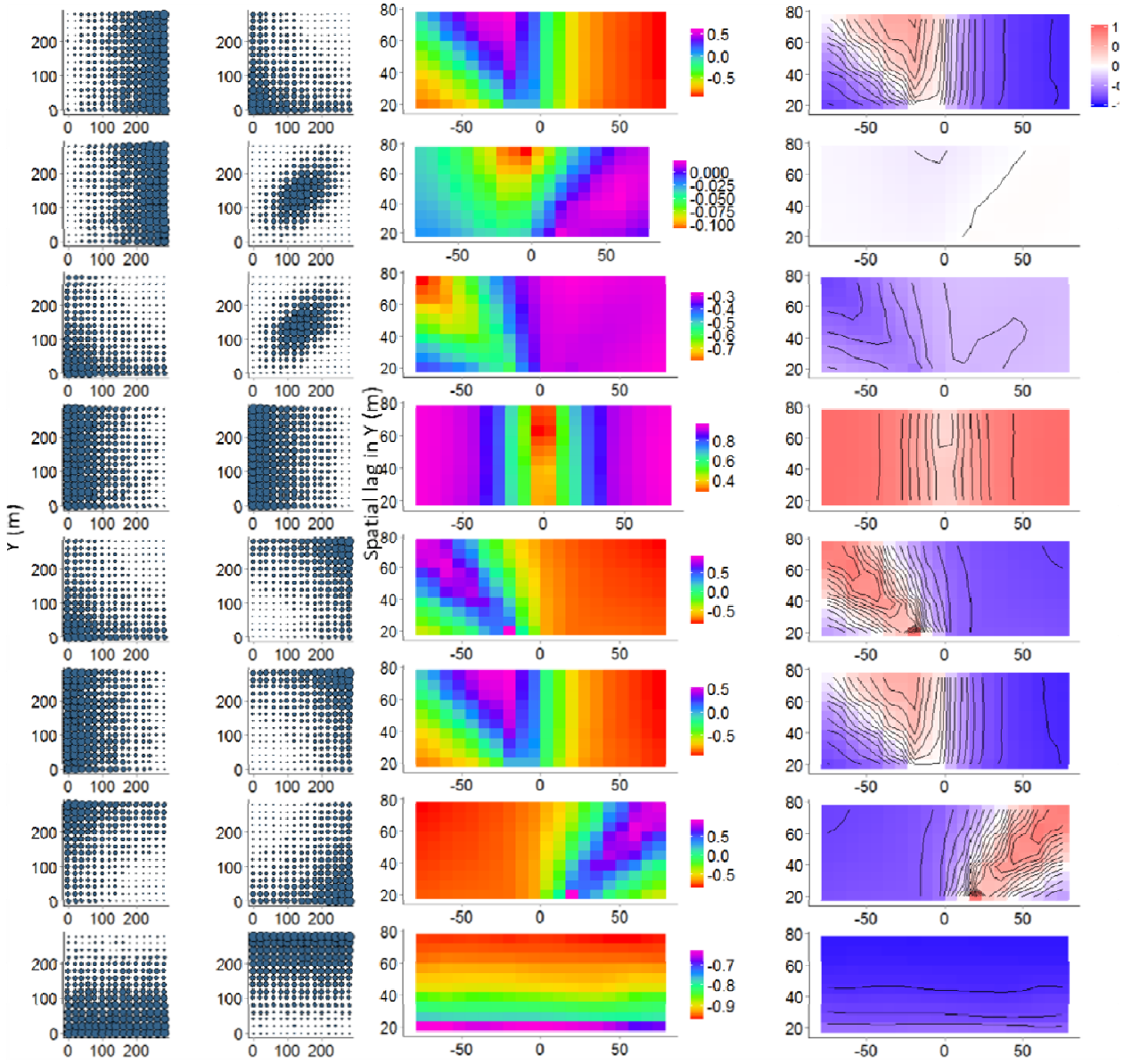
Y (m)
Spatial lag in Y (m)
0 100 200
-50 0 50
20 40 60 80
0.5 0.0 -0.5
0.000 -0.025 -0.050 -0.075 -0.100
-0.3 -0.4 -0.5 -0.6 -0.7
0.8 0.6 0.4
-0.7 -0.8 -0.9

APPENDIX B

We estimated the Type I error rate of the CSR and the toroidal shift models by comparing the observed codispersion values for two CSR species in a 300 × 300-m plot divided into 20 × 20-m grid cells (Figure AB1) with that expected under each of the null models. Here, we present the results from those comparisons. Graphs (Figure AB2) show the values of the (observed – expected) codispersion. Each line in the following tables represents one cell on the codispersion graph. Given are the observed and expected codispersion values; the 'P.value', which is the proportion of values that were the minimum of the number of expected values that were less than or greater than the observed value; the mean of the expected codispersion values and the difference between the observed codispersion value and that mean; and whether or not that difference was significant at the $\alpha = 0.05$ level (two-tailed test).

(a) (b)

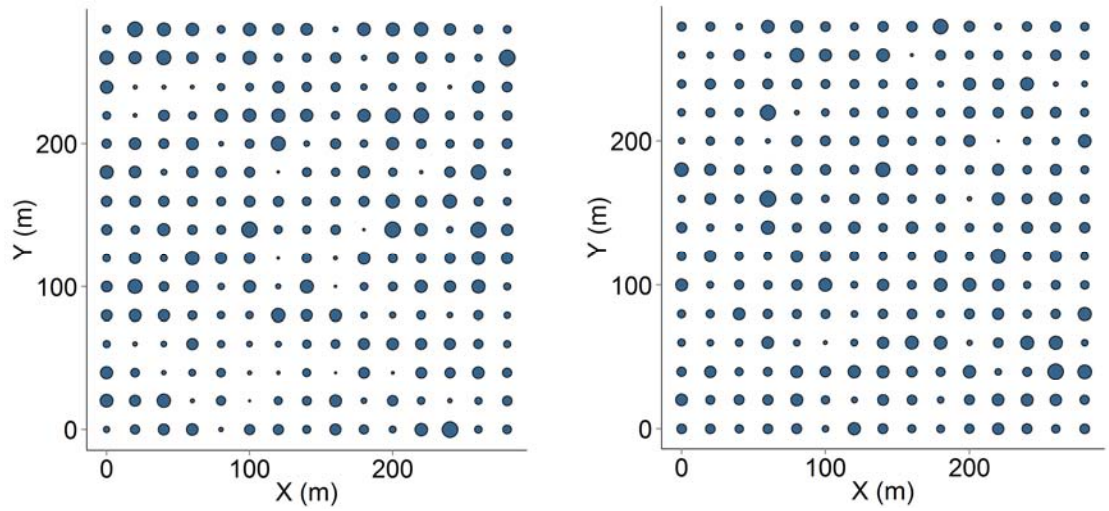

Figure AB1: Simulated relative abundance values of (a) Species 1 and (b) Species 2 used to calculate observed codispersion values that were compared to those generated under the CSR and toroidal shift null models.

(a) (b)

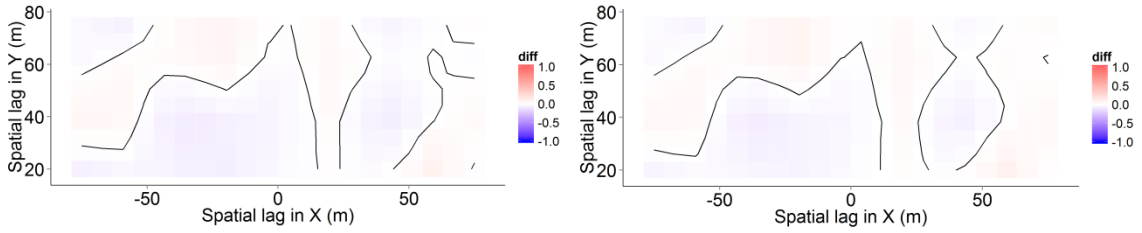

Figure AB2: Observed – expected codispersion for the (a) CSR and (b) toroidal shift null models.

Table AB1: Cell-level results for codispersion analysis with (a) CSR and (b) toroidal shift null models.

(a) CSR null model							
cell	**xx**	**yy**	**Codispersion**	**P.value**	**null_mean**	**diff**	**P.value.cat**
1	-75	20	-0.048	0.271	0.008	-0.057	Non-sig.
2	-67.1	20	-0.039	0.302	0.007	-0.046	Non-sig.
3	-59.2	20	-0.027	0.367	0.005	-0.033	Non-sig.
4	-51.3	20	-0.032	0.296	0.007	-0.039	Non-sig.
5	-43.4	20	-0.036	0.291	0.007	-0.043	Non-sig.
6	-35.5	20	-0.047	0.246	0.006	-0.054	Non-sig.
7	-27.6	20	-0.055	0.191	0.005	-0.06	Non-sig.
8	-19.7	20	-0.065	0.166	0.003	-0.068	Non-sig.
9	-11.8	20	-0.046	0.246	0.002	-0.048	Non-sig.
10	-3.9	20	-0.034	0.312	0.001	-0.035	Non-sig.
11	3.9	20	-0.014	0.397	0.002	-0.016	Non-sig.
12	11.8	20	-0.003	0.467	0.004	-0.006	Non-sig.
13	19.7	20	0.014	0.447	0.006	0.008	Non-sig.
14	27.6	20	-0.002	0.482	0.006	-0.008	Non-sig.
15	35.5	20	-0.015	0.437	0.005	-0.02	Non-sig.
16	43.4	20	0.001	0.487	0.004	-0.003	Non-sig.
17	51.3	20	0.039	0.332	0.004	0.034	Non-sig.
18	59.2	20	0.089	0.171	0.004	0.085	Non-sig.
19	67.1	20	0.042	0.347	0.006	0.037	Non-sig.
20	75	20	0.001	0.427	0.007	-0.006	Non-sig.
21	-75	26.1	-0.008	0.452	0.004	-0.012	Non-sig.
22	-67.1	26.1	-0.003	0.462	0.004	-0.007	Non-sig.
23	-59.2	26.1	0	0.497	0.004	-0.004	Non-sig.
24	-51.3	26.1	-0.026	0.342	0.004	-0.03	Non-sig.
25	-43.4	26.1	-0.045	0.246	0.004	-0.049	Non-sig.
26	-35.5	26.1	-0.061	0.201	0.004	-0.065	Non-sig.
27	-27.6	26.1	-0.062	0.186	0.003	-0.065	Non-sig.
28	-19.7	26.1	-0.062	0.191	0.002	-0.064	Non-sig.
29	-11.8	26.1	-0.048	0.241	0.001	-0.049	Non-sig.
30	-3.9	26.1	-0.038	0.296	0.001	-0.039	Non-sig.
31	3.9	26.1	-0.019	0.372	0.002	-0.02	Non-sig.
32	11.8	26.1	-0.004	0.452	0.003	-0.007	Non-sig.
33	19.7	26.1	0.018	0.447	0.005	0.013	Non-sig.
34	27.6	26.1	-0.009	0.452	0.005	-0.013	Non-sig.
35	35.5	26.1	-0.029	0.357	0.004	-0.033	Non-sig.
36	43.4	26.1	-0.025	0.367	0.004	-0.028	Non-sig.
37	51.3	26.1	0.01	0.477	0.004	0.006	Non-sig.
38	59.2	26.1	0.056	0.256	0.005	0.051	Non-sig.
39	67.1	26.1	0.036	0.362	0.006	0.03	Non-sig.
40	75	26.1	0.015	0.477	0.006	0.009	Non-sig.
41	-75	32.2	0.016	0.457	0.002	0.014	Non-sig.
42	-67.1	32.2	0.02	0.437	0.002	0.017	Non-sig.
43	-59.2	32.2	0.016	0.437	0.003	0.014	Non-sig.
44	-51.3	32.2	-0.022	0.387	0.002	-0.024	Non-sig.
45	-43.4	32.2	-0.05	0.256	0.002	-0.053	Non-sig.
46	-35.5	32.2	-0.069	0.191	0.002	-0.071	Non-sig.
47	-27.6	32.2	-0.065	0.191	0.002	-0.067	Non-sig.
48	-19.7	32.2	-0.059	0.186	0.002	-0.061	Non-sig.

49	-11.8	32.2	-0.048	0.246	0.001	-0.049	Non-sig.
50	-3.9	32.2	-0.041	0.291	0.001	-0.042	Non-sig.
51	3.9	32.2	-0.021	0.397	0.001	-0.023	Non-sig.
52	11.8	32.2	-0.005	0.457	0.003	-0.008	Non-sig.
53	19.7	32.2	0.021	0.437	0.005	0.016	Non-sig.
54	27.6	32.2	-0.013	0.432	0.004	-0.017	Non-sig.
55	35.5	32.2	-0.038	0.327	0.003	-0.041	Non-sig.
56	43.4	32.2	-0.041	0.296	0.003	-0.044	Non-sig.
57	51.3	32.2	-0.008	0.432	0.004	-0.012	Non-sig.
58	59.2	32.2	0.035	0.362	0.005	0.03	Non-sig.
59	67.1	32.2	0.032	0.387	0.006	0.027	Non-sig.
60	75	32.2	0.024	0.427	0.006	0.018	Non-sig.
61	-75	38.3	0.051	0.271	-0.001	0.052	Non-sig.
62	-67.1	38.3	0.051	0.256	0	0.051	Non-sig.
63	-59.2	38.3	0.04	0.332	0.001	0.039	Non-sig.
64	-51.3	38.3	-0.016	0.417	0	-0.016	Non-sig.
65	-43.4	38.3	-0.058	0.251	-0.001	-0.058	Non-sig.
66	-35.5	38.3	-0.08	0.176	0	-0.08	Non-sig.
67	-27.6	38.3	-0.07	0.191	0	-0.071	Non-sig.
68	-19.7	38.3	-0.057	0.221	0.001	-0.058	Non-sig.
69	-11.8	38.3	-0.049	0.276	0.001	-0.05	Non-sig.
70	-3.9	38.3	-0.044	0.291	0	-0.045	Non-sig.
71	3.9	38.3	-0.025	0.412	0.001	-0.026	Non-sig.
72	11.8	38.3	-0.007	0.477	0.002	-0.009	Non-sig.
73	19.7	38.3	0.024	0.372	0.004	0.02	Non-sig.
74	27.6	38.3	-0.018	0.387	0.003	-0.021	Non-sig.
75	35.5	38.3	-0.051	0.236	0.002	-0.053	Non-sig.
76	43.4	38.3	-0.064	0.216	0.002	-0.066	Non-sig.
77	51.3	38.3	-0.034	0.302	0.004	-0.038	Non-sig.
78	59.2	38.3	0.005	0.492	0.006	-0.001	Non-sig.
79	67.1	38.3	0.027	0.412	0.006	0.021	Non-sig.
80	75	38.3	0.037	0.372	0.005	0.032	Non-sig.
81	-75	44.4	0.043	0.271	-0.001	0.044	Non-sig.
82	-67.1	44.4	0.049	0.256	0	0.049	Non-sig.
83	-59.2	44.4	0.048	0.307	0.001	0.047	Non-sig.
84	-51.3	44.4	-0.001	0.492	0	-0.001	Non-sig.
85	-43.4	44.4	-0.039	0.322	-0.001	-0.037	Non-sig.
86	-35.5	44.4	-0.053	0.291	-0.001	-0.052	Non-sig.
87	-27.6	44.4	-0.04	0.327	0	-0.04	Non-sig.
88	-19.7	44.4	-0.024	0.392	0.001	-0.024	Non-sig.
89	-11.8	44.4	-0.031	0.332	0.001	-0.033	Non-sig.
90	-3.9	44.4	-0.036	0.307	0.002	-0.038	Non-sig.
91	3.9	44.4	-0.023	0.402	0.002	-0.025	Non-sig.
92	11.8	44.4	-0.001	0.477	0.002	-0.003	Non-sig.
93	19.7	44.4	0.033	0.332	0.003	0.031	Non-sig.
94	27.6	44.4	-0.007	0.462	0.002	-0.009	Non-sig.
95	35.5	44.4	-0.038	0.302	0.002	-0.04	Non-sig.
96	43.4	44.4	-0.054	0.241	0.003	-0.057	Non-sig.
97	51.3	44.4	-0.033	0.332	0.004	-0.036	Non-sig.
98	59.2	44.4	-0.004	0.467	0.005	-0.009	Non-sig.
99	67.1	44.4	0.017	0.457	0.005	0.011	Non-sig.
100	75	44.4	0.028	0.402	0.005	0.023	Non-sig.
101	-75	50.6	0.022	0.362	-0.001	0.022	Non-sig.
102	-67.1	50.6	0.035	0.332	0.001	0.034	Non-sig.
103	-59.2	50.6	0.045	0.307	0.002	0.043	Non-sig.

104	-51.3	50.6	0.008	0.457	0.001	0.008	Non-sig.
105	-43.4	50.6	-0.019	0.417	-0.001	-0.019	Non-sig.
106	-35.5	50.6	-0.026	0.392	-0.001	-0.025	Non-sig.
107	-27.6	50.6	-0.013	0.432	-0.001	-0.013	Non-sig.
108	-19.7	50.6	0.003	0.492	0	0.002	Non-sig.
109	-11.8	50.6	-0.015	0.442	0.002	-0.017	Non-sig.
110	-3.9	50.6	-0.028	0.352	0.003	-0.031	Non-sig.
111	3.9	50.6	-0.019	0.402	0.003	-0.022	Non-sig.
112	11.8	50.6	0.004	0.477	0.003	0.002	Non-sig.
113	19.7	50.6	0.039	0.332	0.001	0.038	Non-sig.
114	27.6	50.6	0.005	0.482	0.002	0.003	Non-sig.
115	35.5	50.6	-0.022	0.362	0.002	-0.024	Non-sig.
116	43.4	50.6	-0.038	0.307	0.003	-0.041	Non-sig.
117	51.3	50.6	-0.021	0.367	0.004	-0.025	Non-sig.
118	59.2	50.6	0.001	0.492	0.005	-0.004	Non-sig.
119	67.1	50.6	0.011	0.477	0.005	0.005	Non-sig.
120	75	50.6	0.015	0.482	0.005	0.01	Non-sig.
121	-75	56.7	-0.002	0.497	0.001	-0.003	Non-sig.
122	-67.1	56.7	0.018	0.407	0.002	0.017	Non-sig.
123	-59.2	56.7	0.041	0.342	0.003	0.038	Non-sig.
124	-51.3	56.7	0.02	0.412	0.001	0.018	Non-sig.
125	-43.4	56.7	0.003	0.492	0	0.003	Non-sig.
126	-35.5	56.7	0.005	0.472	0	0.006	Non-sig.
127	-27.6	56.7	0.018	0.407	0	0.019	Non-sig.
128	-19.7	56.7	0.033	0.352	0	0.034	Non-sig.
129	-11.8	56.7	0.005	0.477	0.003	0.002	Non-sig.
130	-3.9	56.7	-0.017	0.392	0.005	-0.021	Non-sig.
131	3.9	56.7	-0.014	0.402	0.005	-0.019	Non-sig.
132	11.8	56.7	0.011	0.437	0.003	0.008	Non-sig.
133	19.7	56.7	0.046	0.291	0	0.046	Non-sig.
134	27.6	56.7	0.017	0.412	0.002	0.016	Non-sig.
135	35.5	56.7	-0.005	0.442	0.003	-0.007	Non-sig.
136	43.4	56.7	-0.02	0.392	0.004	-0.023	Non-sig.
137	51.3	56.7	-0.009	0.417	0.004	-0.012	Non-sig.
138	59.2	56.7	0.005	0.492	0.004	0.002	Non-sig.
139	67.1	56.7	0.004	0.482	0.005	-0.001	Non-sig.
140	75	56.7	0	0.447	0.006	-0.005	Non-sig.
141	-75	62.8	-0.025	0.372	0.003	-0.028	Non-sig.
142	-67.1	62.8	-0.01	0.452	0.003	-0.013	Non-sig.
143	-59.2	62.8	0.012	0.462	0.004	0.008	Non-sig.
144	-51.3	62.8	0.019	0.417	0.003	0.016	Non-sig.
145	-43.4	62.8	0.024	0.382	0.002	0.023	Non-sig.
146	-35.5	62.8	0.042	0.291	0.001	0.041	Non-sig.
147	-27.6	62.8	0.054	0.271	0.001	0.053	Non-sig.
148	-19.7	62.8	0.067	0.236	0.001	0.066	Non-sig.
149	-11.8	62.8	0.03	0.367	0.004	0.026	Non-sig.
150	-3.9	62.8	0.001	0.472	0.006	-0.005	Non-sig.
151	3.9	62.8	-0.005	0.452	0.006	-0.011	Non-sig.
152	11.8	62.8	0.018	0.397	0.003	0.014	Non-sig.
153	19.7	62.8	0.049	0.246	0	0.049	Non-sig.
154	27.6	62.8	0.023	0.397	0.002	0.021	Non-sig.
155	35.5	62.8	0.004	0.497	0.004	0	Non-sig.
156	43.4	62.8	-0.011	0.417	0.005	-0.016	Non-sig.
157	51.3	62.8	-0.004	0.467	0.004	-0.008	Non-sig.
158	59.2	62.8	0.006	0.487	0.003	0.003	Non-sig.

159	67.1	62.8	0.001	0.452	0.005	-0.004	Non-sig.
160	75	62.8	-0.005	0.417	0.007	-0.011	Non-sig.
161	-75	68.9	-0.022	0.367	0.004	-0.026	Non-sig.
162	-67.1	68.9	-0.023	0.377	0.004	-0.027	Non-sig.
163	-59.2	68.9	-0.019	0.407	0.004	-0.023	Non-sig.
164	-51.3	68.9	0.004	0.492	0.003	0.001	Non-sig.
165	-43.4	68.9	0.02	0.417	0.002	0.018	Non-sig.
166	-35.5	68.9	0.045	0.286	0.002	0.043	Non-sig.
167	-27.6	68.9	0.056	0.241	0.002	0.054	Non-sig.
168	-19.7	68.9	0.068	0.221	0.003	0.065	Non-sig.
169	-11.8	68.9	0.033	0.357	0.005	0.028	Non-sig.
170	-3.9	68.9	0.007	0.482	0.006	0.001	Non-sig.
171	3.9	68.9	-0.001	0.462	0.005	-0.006	Non-sig.
172	11.8	68.9	0.018	0.417	0.004	0.014	Non-sig.
173	19.7	68.9	0.043	0.271	0.002	0.042	Non-sig.
174	27.6	68.9	0.014	0.462	0.003	0.011	Non-sig.
175	35.5	68.9	-0.007	0.442	0.004	-0.011	Non-sig.
176	43.4	68.9	-0.022	0.357	0.005	-0.028	Non-sig.
177	51.3	68.9	-0.013	0.417	0.005	-0.017	Non-sig.
178	59.2	68.9	0.001	0.492	0.004	-0.003	Non-sig.
179	67.1	68.9	0.006	0.487	0.006	0	Non-sig.
180	75	68.9	0.009	0.487	0.007	0.002	Non-sig.
181	-75	75	-0.02	0.407	0.005	-0.024	Non-sig.
182	-67.1	75	-0.035	0.327	0.005	-0.039	Non-sig.
183	-59.2	75	-0.047	0.286	0.005	-0.052	Non-sig.
184	-51.3	75	-0.01	0.442	0.003	-0.013	Non-sig.
185	-43.4	75	0.017	0.457	0.003	0.015	Non-sig.
186	-35.5	75	0.048	0.271	0.003	0.046	Non-sig.
187	-27.6	75	0.058	0.231	0.004	0.054	Non-sig.
188	-19.7	75	0.069	0.201	0.005	0.065	Non-sig.
189	-11.8	75	0.036	0.347	0.005	0.03	Non-sig.
190	-3.9	75	0.011	0.467	0.005	0.006	Non-sig.
191	3.9	75	0.003	0.477	0.005	-0.002	Non-sig.
192	11.8	75	0.018	0.437	0.004	0.014	Non-sig.
193	19.7	75	0.038	0.286	0.003	0.036	Non-sig.
194	27.6	75	0.006	0.482	0.004	0.002	Non-sig.
195	35.5	75	-0.017	0.377	0.005	-0.022	Non-sig.
196	43.4	75	-0.033	0.307	0.006	-0.038	Non-sig.
197	51.3	75	-0.021	0.357	0.005	-0.026	Non-sig.
198	59.2	75	-0.004	0.472	0.005	-0.009	Non-sig.
199	67.1	75	0.011	0.462	0.006	0.005	Non-sig.
200	75	75	0.021	0.432	0.008	0.013	Non-sig.
(b) Toroidal shift null model							
cell	**xx**	**yy**	**Codispersion**	**P.value**	**null_mean**	**diff**	**P.value.cat**
1	-75	20	-0.048	0.286	-0.005	-0.043	Non-sig.
2	-67.1	20	-0.039	0.337	-0.006	-0.032	Non-sig.
3	-59.2	20	-0.027	0.442	-0.008	-0.019	Non-sig.
4	-51.3	20	-0.032	0.407	-0.006	-0.026	Non-sig.
5	-43.4	20	-0.036	0.347	-0.005	-0.031	Non-sig.
6	-35.5	20	-0.047	0.312	-0.007	-0.04	Non-sig.
7	-27.6	20	-0.055	0.256	-0.011	-0.045	Non-sig.
8	-19.7	20	-0.065	0.256	-0.015	-0.051	Non-sig.
9	-11.8	20	-0.046	0.276	-0.009	-0.037	Non-sig.
10	-3.9	20	-0.034	0.317	-0.006	-0.028	Non-sig.

11	3.9	20	-0.014	0.402	-0.004	-0.01	Non-sig.
12	11.8	20	-0.003	0.487	-0.004	0.001	Non-sig.
13	19.7	20	0.014	0.412	-0.004	0.019	Non-sig.
14	27.6	20	-0.002	0.457	-0.005	0.003	Non-sig.
15	35.5	20	-0.015	0.447	-0.006	-0.009	Non-sig.
16	43.4	20	0.001	0.447	-0.006	0.007	Non-sig.
17	51.3	20	0.039	0.251	-0.005	0.043	Non-sig.
18	59.2	20	0.089	0.116	-0.003	0.093	Non-sig.
19	67.1	20	0.042	0.261	-0.005	0.047	Non-sig.
20	75	20	0.001	0.437	-0.006	0.006	Non-sig.
21	-75	26.1	-0.008	0.432	-0.002	-0.006	Non-sig.
22	-67.1	26.1	-0.003	0.467	-0.003	0	Non-sig.
23	-59.2	26.1	0	0.487	-0.003	0.003	Non-sig.
24	-51.3	26.1	-0.026	0.377	-0.004	-0.022	Non-sig.
25	-43.4	26.1	-0.045	0.241	-0.004	-0.041	Non-sig.
26	-35.5	26.1	-0.061	0.206	-0.007	-0.054	Non-sig.
27	-27.6	26.1	-0.062	0.216	-0.009	-0.052	Non-sig.
28	-19.7	26.1	-0.062	0.231	-0.013	-0.049	Non-sig.
29	-11.8	26.1	-0.048	0.246	-0.009	-0.038	Non-sig.
30	-3.9	26.1	-0.038	0.327	-0.007	-0.031	Non-sig.
31	3.9	26.1	-0.019	0.412	-0.005	-0.013	Non-sig.
32	11.8	26.1	-0.004	0.447	-0.005	0.001	Non-sig.
33	19.7	26.1	0.018	0.362	-0.005	0.023	Non-sig.
34	27.6	26.1	-0.009	0.492	-0.006	-0.002	Non-sig.
35	35.5	26.1	-0.029	0.397	-0.007	-0.022	Non-sig.
36	43.4	26.1	-0.025	0.417	-0.007	-0.018	Non-sig.
37	51.3	26.1	0.01	0.402	-0.006	0.016	Non-sig.
38	59.2	26.1	0.056	0.206	-0.004	0.06	Non-sig.
39	67.1	26.1	0.036	0.302	-0.005	0.041	Non-sig.
40	75	26.1	0.015	0.387	-0.005	0.021	Non-sig.
41	-75	32.2	0.016	0.432	0	0.017	Non-sig.
42	-67.1	32.2	0.02	0.412	0	0.02	Non-sig.
43	-59.2	32.2	0.016	0.407	-0.001	0.017	Non-sig.
44	-51.3	32.2	-0.022	0.362	-0.002	-0.02	Non-sig.
45	-43.4	32.2	-0.05	0.246	-0.003	-0.047	Non-sig.
46	-35.5	32.2	-0.069	0.176	-0.007	-0.062	Non-sig.
47	-27.6	32.2	-0.065	0.206	-0.009	-0.057	Non-sig.
48	-19.7	32.2	-0.059	0.261	-0.011	-0.048	Non-sig.
49	-11.8	32.2	-0.048	0.271	-0.009	-0.039	Non-sig.
50	-3.9	32.2	-0.041	0.332	-0.008	-0.033	Non-sig.
51	3.9	32.2	-0.021	0.447	-0.006	-0.015	Non-sig.
52	11.8	32.2	-0.005	0.447	-0.006	0.001	Non-sig.
53	19.7	32.2	0.021	0.412	-0.005	0.026	Non-sig.
54	27.6	32.2	-0.013	0.447	-0.007	-0.006	Non-sig.
55	35.5	32.2	-0.038	0.332	-0.008	-0.03	Non-sig.
56	43.4	32.2	-0.041	0.312	-0.008	-0.033	Non-sig.
57	51.3	32.2	-0.008	0.482	-0.006	-0.002	Non-sig.
58	59.2	32.2	0.035	0.302	-0.005	0.04	Non-sig.
59	67.1	32.2	0.032	0.317	-0.005	0.037	Non-sig.
60	75	32.2	0.024	0.377	-0.005	0.03	Non-sig.
61	-75	38.3	0.051	0.286	0.002	0.049	Non-sig.
62	-67.1	38.3	0.051	0.296	0.003	0.048	Non-sig.
63	-59.2	38.3	0.04	0.352	0.003	0.037	Non-sig.
64	-51.3	38.3	-0.016	0.367	0	-0.016	Non-sig.
65	-43.4	38.3	-0.058	0.236	-0.002	-0.056	Non-sig.

66	-35.5	38.3	-0.08	0.151	-0.006	-0.074	Non-sig.
67	-27.6	38.3	-0.07	0.201	-0.008	-0.062	Non-sig.
68	-19.7	38.3	-0.057	0.276	-0.01	-0.047	Non-sig.
69	-11.8	38.3	-0.049	0.312	-0.009	-0.04	Non-sig.
70	-3.9	38.3	-0.044	0.352	-0.009	-0.036	Non-sig.
71	3.9	38.3	-0.025	0.392	-0.008	-0.017	Non-sig.
72	11.8	38.3	-0.007	0.472	-0.007	0	Non-sig.
73	19.7	38.3	0.024	0.392	-0.006	0.03	Non-sig.
74	27.6	38.3	-0.018	0.397	-0.007	-0.011	Non-sig.
75	35.5	38.3	-0.051	0.307	-0.008	-0.042	Non-sig.
76	43.4	38.3	-0.064	0.256	-0.009	-0.055	Non-sig.
77	51.3	38.3	-0.034	0.402	-0.007	-0.027	Non-sig.
78	59.2	38.3	0.005	0.432	-0.005	0.011	Non-sig.
79	67.1	38.3	0.027	0.327	-0.005	0.032	Non-sig.
80	75	38.3	0.037	0.312	-0.005	0.042	Non-sig.
81	-75	44.4	0.043	0.312	0.002	0.04	Non-sig.
82	-67.1	44.4	0.049	0.322	0.003	0.046	Non-sig.
83	-59.2	44.4	0.048	0.347	0.004	0.044	Non-sig.
84	-51.3	44.4	-0.001	0.462	0.001	-0.002	Non-sig.
85	-43.4	44.4	-0.039	0.296	-0.002	-0.037	Non-sig.
86	-35.5	44.4	-0.053	0.261	-0.005	-0.048	Non-sig.
87	-27.6	44.4	-0.04	0.322	-0.006	-0.034	Non-sig.
88	-19.7	44.4	-0.024	0.397	-0.007	-0.016	Non-sig.
89	-11.8	44.4	-0.031	0.382	-0.007	-0.024	Non-sig.
90	-3.9	44.4	-0.036	0.367	-0.007	-0.029	Non-sig.
91	3.9	44.4	-0.023	0.392	-0.006	-0.016	Non-sig.
92	11.8	44.4	-0.001	0.477	-0.006	0.005	Non-sig.
93	19.7	44.4	0.033	0.382	-0.005	0.038	Non-sig.
94	27.6	44.4	-0.007	0.467	-0.006	-0.001	Non-sig.
95	35.5	44.4	-0.038	0.327	-0.007	-0.031	Non-sig.
96	43.4	44.4	-0.054	0.231	-0.008	-0.046	Non-sig.
97	51.3	44.4	-0.033	0.337	-0.008	-0.025	Non-sig.
98	59.2	44.4	-0.004	0.462	-0.007	0.003	Non-sig.
99	67.1	44.4	0.017	0.352	-0.005	0.022	Non-sig.
100	75	44.4	0.028	0.342	-0.004	0.032	Non-sig.
101	-75	50.6	0.022	0.437	0.001	0.02	Non-sig.
102	-67.1	50.6	0.035	0.377	0.002	0.032	Non-sig.
103	-59.2	50.6	0.045	0.342	0.003	0.041	Non-sig.
104	-51.3	50.6	0.008	0.467	0	0.008	Non-sig.
105	-43.4	50.6	-0.019	0.387	-0.002	-0.017	Non-sig.
106	-35.5	50.6	-0.026	0.367	-0.004	-0.022	Non-sig.
107	-27.6	50.6	-0.013	0.427	-0.005	-0.008	Non-sig.
108	-19.7	50.6	0.003	0.427	-0.006	0.008	Non-sig.
109	-11.8	50.6	-0.015	0.447	-0.005	-0.01	Non-sig.
110	-3.9	50.6	-0.028	0.402	-0.005	-0.022	Non-sig.
111	3.9	50.6	-0.019	0.432	-0.005	-0.014	Non-sig.
112	11.8	50.6	0.004	0.442	-0.004	0.009	Non-sig.
113	19.7	50.6	0.039	0.322	-0.004	0.043	Non-sig.
114	27.6	50.6	0.005	0.462	-0.005	0.01	Non-sig.
115	35.5	50.6	-0.022	0.372	-0.006	-0.016	Non-sig.
116	43.4	50.6	-0.038	0.291	-0.007	-0.031	Non-sig.
117	51.3	50.6	-0.021	0.407	-0.008	-0.013	Non-sig.
118	59.2	50.6	0.001	0.457	-0.009	0.009	Non-sig.
119	67.1	50.6	0.011	0.412	-0.006	0.016	Non-sig.
120	75	50.6	0.015	0.392	-0.004	0.019	Non-sig.

121	-75	56.7	-0.002	0.432	0	-0.003	Non-sig.
122	-67.1	56.7	0.018	0.422	0.001	0.017	Non-sig.
123	-59.2	56.7	0.041	0.372	0.002	0.038	Non-sig.
124	-51.3	56.7	0.02	0.397	0	0.019	Non-sig.
125	-43.4	56.7	0.003	0.467	-0.002	0.005	Non-sig.
126	-35.5	56.7	0.005	0.437	-0.004	0.009	Non-sig.
127	-27.6	56.7	0.018	0.342	-0.004	0.022	Non-sig.
128	-19.7	56.7	0.033	0.281	-0.004	0.037	Non-sig.
129	-11.8	56.7	0.005	0.397	-0.003	0.008	Non-sig.
130	-3.9	56.7	-0.017	0.437	-0.003	-0.014	Non-sig.
131	3.9	56.7	-0.014	0.432	-0.003	-0.011	Non-sig.
132	11.8	56.7	0.011	0.422	-0.003	0.014	Non-sig.
133	19.7	56.7	0.046	0.271	-0.003	0.049	Non-sig.
134	27.6	56.7	0.017	0.367	-0.004	0.021	Non-sig.
135	35.5	56.7	-0.005	0.487	-0.004	0	Non-sig.
136	43.4	56.7	-0.02	0.382	-0.006	-0.014	Non-sig.
137	51.3	56.7	-0.009	0.482	-0.008	-0.001	Non-sig.
138	59.2	56.7	0.005	0.427	-0.01	0.015	Non-sig.
139	67.1	56.7	0.004	0.447	-0.006	0.01	Non-sig.
140	75	56.7	0	0.467	-0.003	0.003	Non-sig.
141	-75	62.8	-0.025	0.337	-0.001	-0.024	Non-sig.
142	-67.1	62.8	-0.01	0.417	-0.001	-0.009	Non-sig.
143	-59.2	62.8	0.012	0.452	-0.001	0.013	Non-sig.
144	-51.3	62.8	0.019	0.372	-0.001	0.02	Non-sig.
145	-43.4	62.8	0.024	0.357	-0.001	0.025	Non-sig.
146	-35.5	62.8	0.042	0.276	-0.001	0.043	Non-sig.
147	-27.6	62.8	0.054	0.241	-0.001	0.055	Non-sig.
148	-19.7	62.8	0.067	0.206	-0.001	0.069	Non-sig.
149	-11.8	62.8	0.03	0.302	-0.001	0.03	Non-sig.
150	-3.9	62.8	0.001	0.457	0	0.001	Non-sig.
151	3.9	62.8	-0.005	0.492	0	-0.005	Non-sig.
152	11.8	62.8	0.018	0.382	-0.001	0.019	Non-sig.
153	19.7	62.8	0.049	0.241	-0.002	0.05	Non-sig.
154	27.6	62.8	0.023	0.362	-0.003	0.026	Non-sig.
155	35.5	62.8	0.004	0.467	-0.003	0.007	Non-sig.
156	43.4	62.8	-0.011	0.472	-0.005	-0.005	Non-sig.
157	51.3	62.8	-0.004	0.457	-0.008	0.004	Non-sig.
158	59.2	62.8	0.006	0.432	-0.01	0.016	Non-sig.
159	67.1	62.8	0.001	0.482	-0.006	0.007	Non-sig.
160	75	62.8	-0.005	0.487	-0.003	-0.002	Non-sig.
161	-75	68.9	-0.022	0.362	-0.002	-0.02	Non-sig.
162	-67.1	68.9	-0.023	0.357	-0.003	-0.02	Non-sig.
163	-59.2	68.9	-0.019	0.372	-0.003	-0.016	Non-sig.
164	-51.3	68.9	0.004	0.452	-0.002	0.005	Non-sig.
165	-43.4	68.9	0.02	0.387	-0.001	0.021	Non-sig.
166	-35.5	68.9	0.045	0.241	0	0.045	Non-sig.
167	-27.6	68.9	0.056	0.236	0	0.056	Non-sig.
168	-19.7	68.9	0.068	0.206	0	0.068	Non-sig.
169	-11.8	68.9	0.033	0.296	0	0.033	Non-sig.
170	-3.9	68.9	0.007	0.437	0	0.007	Non-sig.
171	3.9	68.9	-0.001	0.452	0	0	Non-sig.
172	11.8	68.9	0.018	0.367	-0.001	0.018	Non-sig.
173	19.7	68.9	0.043	0.286	-0.001	0.044	Non-sig.
174	27.6	68.9	0.014	0.392	-0.003	0.017	Non-sig.
175	35.5	68.9	-0.007	0.482	-0.004	-0.003	Non-sig.

176	43.4	68.9	-0.022	0.407	-0.006	-0.016	Non-sig.
177	51.3	68.9	-0.013	0.487	-0.007	-0.005	Non-sig.
178	59.2	68.9	0.001	0.432	-0.009	0.01	Non-sig.
179	67.1	68.9	0.006	0.442	-0.006	0.012	Non-sig.
180	75	68.9	0.009	0.482	-0.003	0.012	Non-sig.
181	-75	75	-0.02	0.402	-0.002	-0.017	Non-sig.
182	-67.1	75	-0.035	0.307	-0.004	-0.031	Non-sig.
183	-59.2	75	-0.047	0.281	-0.005	-0.042	Non-sig.
184	-51.3	75	-0.01	0.472	-0.002	-0.008	Non-sig.
185	-43.4	75	0.017	0.387	0	0.017	Non-sig.
186	-35.5	75	0.048	0.266	0.002	0.047	Non-sig.
187	-27.6	75	0.058	0.226	0.002	0.056	Non-sig.
188	-19.7	75	0.069	0.226	0.001	0.068	Non-sig.
189	-11.8	75	0.036	0.312	0.001	0.035	Non-sig.
190	-3.9	75	0.011	0.387	0	0.011	Non-sig.
191	3.9	75	0.003	0.427	-0.001	0.003	Non-sig.
192	11.8	75	0.018	0.372	-0.001	0.018	Non-sig.
193	19.7	75	0.038	0.302	-0.001	0.039	Non-sig.
194	27.6	75	0.006	0.457	-0.003	0.009	Non-sig.
195	35.5	75	-0.017	0.462	-0.005	-0.012	Non-sig.
196	43.4	75	-0.033	0.422	-0.007	-0.026	Non-sig.
197	51.3	75	-0.021	0.437	-0.007	-0.014	Non-sig.
198	59.2	75	-0.004	0.472	-0.008	0.003	Non-sig.
199	67.1	75	0.011	0.442	-0.006	0.017	Non-sig.
200	75	75	0.021	0.387	-0.004	0.025	Non-sig.

APPENDIX C

We tested the effects of detrending on the estimation of the observed and expected codispersion using a trend surface linear regression (abundance ~ X + Y) on the abundance rasters for two of the simulated abundance datasets (Figure 1). The residuals from these trend surface regressions were then used in a codispersion analysis. The results from this analysis show that detrending removes interesting spatial pattern from the data (Figure 2), which results in codispersion values near to zero (Figure 3).

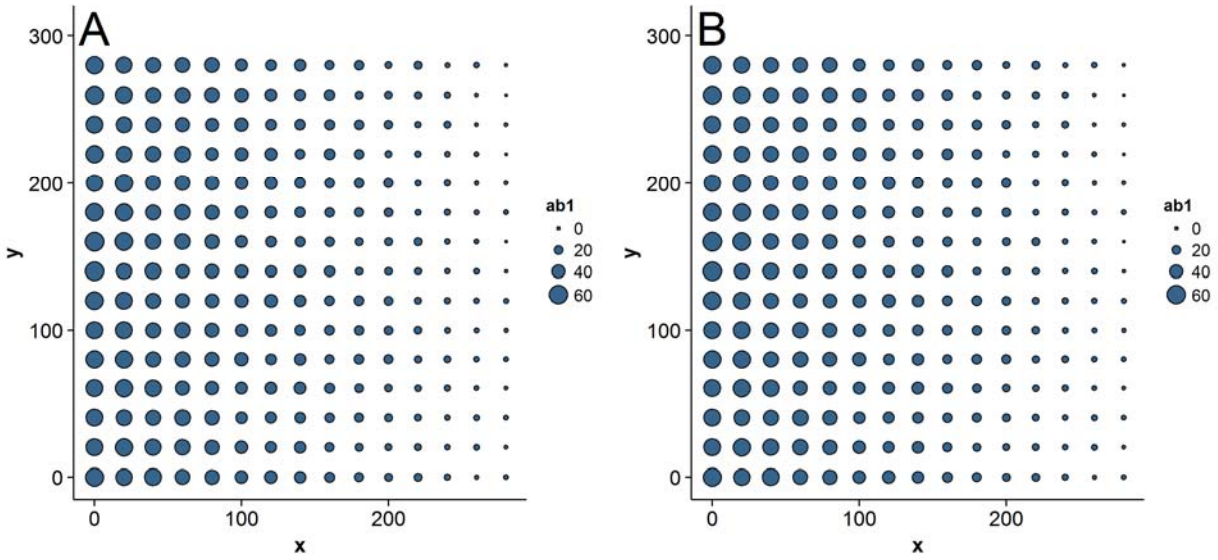

Figure 1. Simulated abundance patterns for two species in 20 × 20-m grid cells in a 300 × 300-m plot.

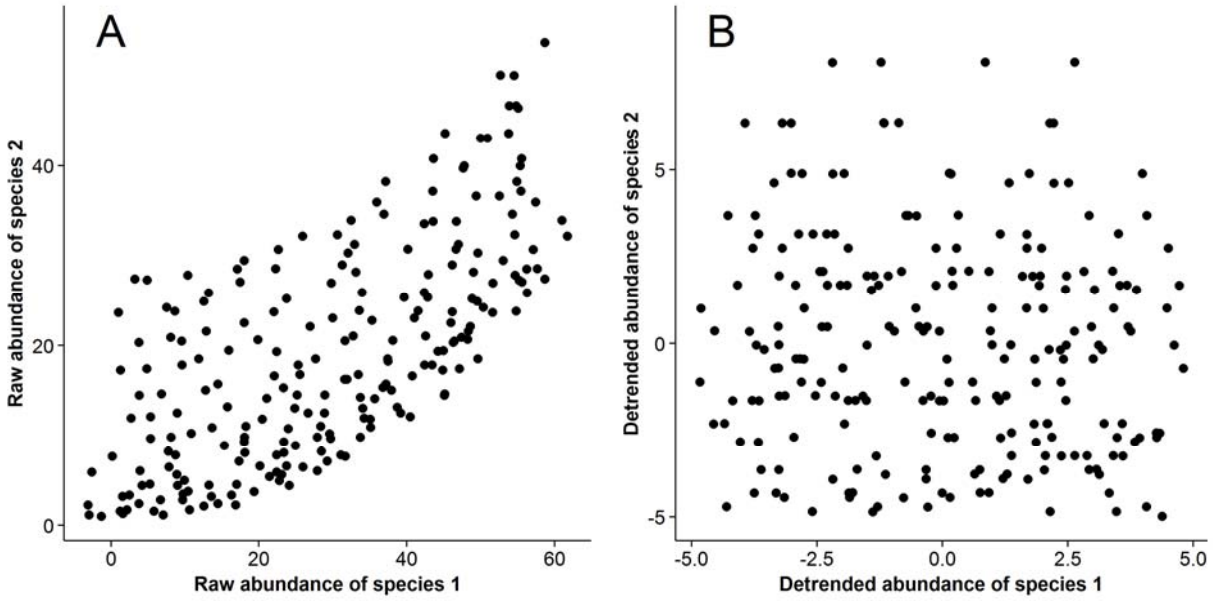

Figure 2. Scatterplots showing the relationship between the (A) raw and (B) detrended simulated abundance values in 20 × 20-m grid cells in a 300 × 300-m plot.

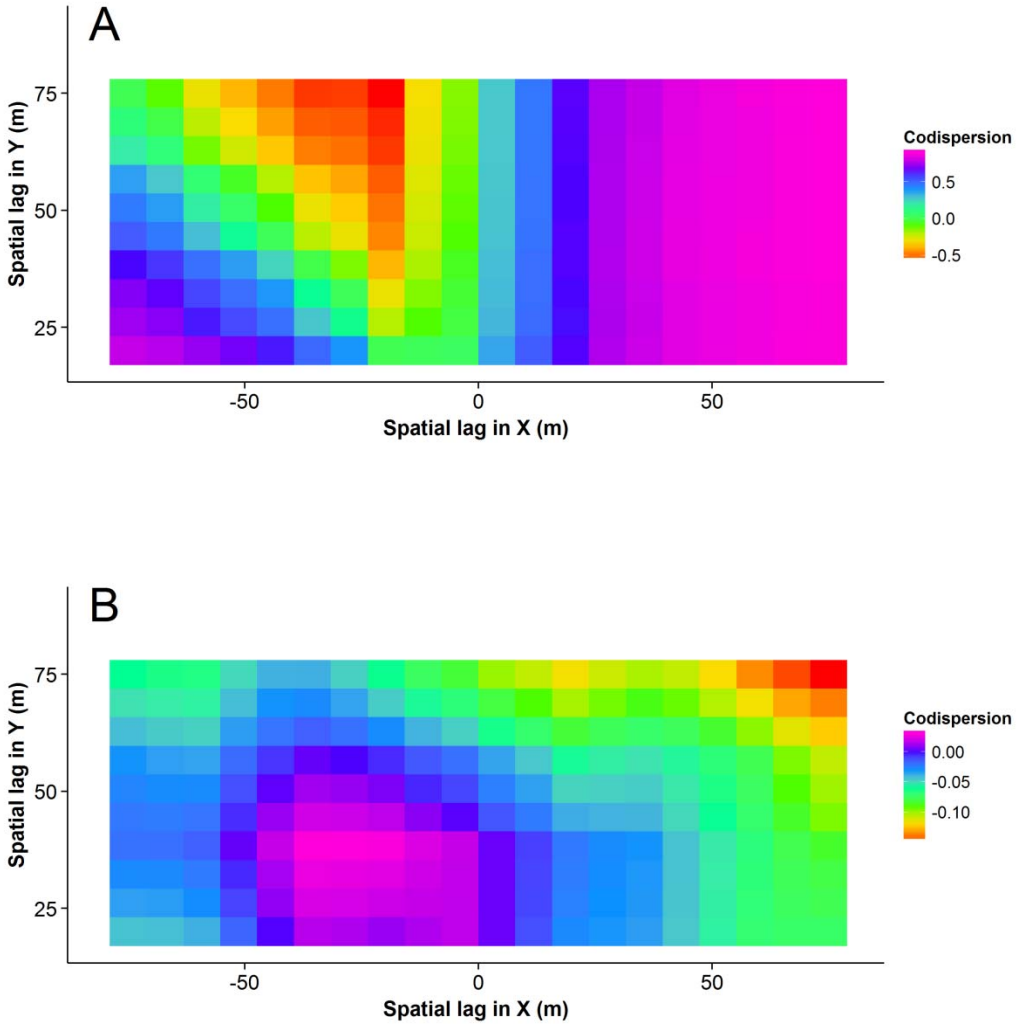

Figure 3. Codispersion plots for the simulated species co-occurrence patterns in 20 × 20-m grid cells in a 300 × 300-m plot. A: raw data; B: detrended data.